Geomechanics and Engineering, *Vol. 26, No. 6 (2021) 551-563*
https://doi.org/10.12989/gae.2021.26.6.551

Strain performance and fracture response characteristics of hard rock under cyclic disturbance loading

Yun Cheng[*1,2], Zhanping Song[**1,2], Wanxue Song[1], Shuguang Li[2,3], Tengtian Yang[2,4], Zekun Zhang[1], Tong Wang[1] and Kuisheng Wang[1]

[1]*School of Civil Engineering, Xi'an University of Architecture and Technology, Xi'an 710055, China*
[2]*Shaanxi Key Lab of Geotechnical and Underground Space Engineering, Xi'an 710055, China*
[3]*Post-Doctoral Research Workstation, China Railway 20th Bureau Group Co. Ltd., Xi'an, 710016, China*
[4]*China Railway Bridge Engineering Bureau Group Co. Ltd., Tianjin 300300, China*

(Received August 9, 2021, Revised September 10, 2021, Accepted September 23, 2021)

Abstract. Fracture characteristics and damage mechanism of rock mass under cyclic loading and unloading is one of the basic research topics of rock mechanics. To study the deformation and fracture response characteristics of brittle hard rock under cyclic disturbance loading, cyclic loading and unloading tests were carried out at different loading and unloading rates, and the stress-strain curve shapes, modulus elastic, critical damage value, fracture characteristics and fractal dimension laws were analyzed. The results show that the loading and unloading effect has significant influence on stress-strain curve shape and fatigue life. The hysteresis loop is overdistributed from sparse to dense with increasing loading and unloading rate and fatigue life is significantly reduced. The loading and unloading action has a phased control effect on peak strength with a first increases and then decreases. The rock has a stable rupture type with a brittle strength about 1.16~31.07% of peak strength, and brittle strength indicates a brittle fracture. With increasing cycle number, loading elastic modulus and unloading elastic modulus firstly increase sharply then increase linearly and finally decrease gradually. The critical damage factor has an approximately linear relationship with loading and unloading rates. The rock mainly occurs oblique shear through and tension through ruptures, and the failure types changes from shear failure to tension failure excessively with increasing loading and unloading rate. The increased loading and unloading rate weakens the end constraint effect, the greater the loading and unloading rate, the more obvious the fragmentation degree, and the more significant the fragments uniformity. The fractal dimension is logarithmic function related to loading and unloading rate.

Keywords: fractal dimension; fracture response characteristic; hard rock; loading and unloading effect; peak strength

1. Introduction

Mechanical characteristics and long-term stability of rock mass under complex stress environment has gradually attracted the attention with the strategy implementation of deep exploitation in field of geotechnical and mining engineering to seek space and resources from deep rock mass (Bahaaddini *et al.* 2013, Kim *et al.* 2019, Fan *et al.* 2020). Especially in the aspects of rock mass excavation and deformation evolution (Bahrani *et al.* 2016, Wu *et al.* 2020, Cheng *et al.* 2020a, Capuani and Willis 1997, Song *et al.* 2020), long-term stability during rock mass unloading is affected by mechanical excavation and vibration loading, and its stability characteristics is closely related to dynamic stress level and disturbance frequency. In stress disturbance environment, excavation disturbance effect often causes structure adjustment and internal stress redistribution (Wu *et al.* 2021a, b, c), and even induces strength deterioration (Li *et al.* 2016, Zhou *et al.* 2020, Zhao *et al.* 2021). Therefore, cycle dynamics disturbance is very likely to be the main cause of disasters frequent occurrence such as mechanical property deterioration and instability fracture of engineering rock mass.

Aiming at the mechanical characteristics of one-time failure, many scholars have carried out uniaxial and triaxial mechanical failure tests (Song *et al.* 2020, Bahrani and Kaiser 2016, Bahaaddini *et al.* 2013), and dynamic mechanical tests under explosion and impact loads (Cheng *et al.* 2020b, Capuani and Willis 1997), which have revealed in detail the correlation between mechanical parameters and failure modes. However, dynamic disturbance under cyclic loading is substantially similar to rock mass excavation and unloading effect, making the rock mass have different mechanical responses in loading and unloading process, such as strain softening and hardening effect, acceleration effect of strength and difference in fracture mode and crushing forms, which are ultimately related to stress disturbance parameters and loading and unloading rates. Taheri *et al.* (2020) studied the relationship between stress loading effect and mechanical parameters of sandstone. The acceleration rate effect refers to the mechanical behavior changing with loading rate. Li *et al.* (2016) studied the acceleration rate effect of uniaxial

*Corresponding author, Ph.D. Candidate
E-mail: chengyun_ifu@163.com
**Corresponding author, Professor, Ph.D.
E-mail: songzhpyt@xauat.edu.cn

ISSN: 2005-307X (Print), 2092-6219 (Online)

compressive strength of coal; Zhou *et al.* (2020) explored the elastic modulus evolution of chlorite phyllite under cyclic loading tests.

However, evolution law of peak strength under cyclic disturbance loading is not identical due to the differential characteristics in stress loading rate or strain rate and unloading stress path. For this purpose, literature (Qi *et al.* 2009) revealed that the stress loading rate had different leading effects on the mechanical properties, and the peak strength of hard rocks such as limestone, granite, and basalt did not increase with increasing stress loading rate. It can be seen from the above analysis that the evolution laws of peak strength with the increase of stress loading rate are not completely uniform. In particular, high loading and unloading rate or high strain conditions have extremely severe cyclic disturbance on rocks. Affected by special factors such as control modes of loading and unloading, cyclic stress level and unloading rate, mechanical parameters such as peak strength and elastic modulus will appear abnormal performance accordingly.

The main research theme of this paper is to explore the strain and fracture response characteristics of hard rock under cyclic disturbance loading, and then perform the loading and unloading mechanical tests on hard rock at different loading and unloading rates, and clarify the correlation between deformation damage and fracture morphology characteristics. The morphological characteristics of stress-strain curves, peak strain and peak strength characteristics, unloading elastic mode and critical damage evolution laws were discussed, and then the fracture mode and fracture fractal features were analyzed based on experimental results.

2. Experimental materials and methodology

2.1 Sample preparation

The physical and mechanical properties of natural rock masses are significantly different, leading to testing data discreteness under controlled test conditions. Therefore, it is particularly important to carry out relevant tests on prefabricated hard rock based on the similarity principle in laboratory. To obtain the tight and brittle hard rock that meet the test conditions, standard hard rock were prepared according to the weight ratio of 4 : 1 : 0.35 : 0.16 with high strength cement (P·O 42.5), fine quartz sand (100 mesh), high purity iron ore powder (Fe_3O_4) and engineering accelerating agent as similar materials. It should be noted that the brittle hard rock in this study only indicates a similarity in strength.

The casting size of initial hard rock was 300 mm × 400 mm × 100 mm to obtain the homogeneous rock mass, and reduced the discrete type of single rock sample. Use a small - frequency vibrating table to vibrate and compact, and then the core drilling and grinding of standard hard rocks (φ50 mm × 100 mm) were carried out after curing for 120 hours in a humid state, and the non-parallelism and non-perpendicularity of the end faces were less than 0.02 mm. Those standard hard rocks were preserved in wet environment for 23 days, then weighed, and measured the wave velocity, and removed those rock samples with large residual differences. The weight and wave velocities of effective hard rocks with little difference in physical and mechanical characteristics are 400.57~407.10 g and 4.40~5.40 km/s, respectively. Laboratory core drilling and standard hard rocks are shown in Fig.1.

Fig. 1 Hard rocks

Fig. 2 Rock mechanics testing machine

2.2 Experimental equipment and procedure

The cyclic loading and unloading test was completed in the Key Laboratory of Geotechnical and Underground Space Engineering of Shaanxi Province, Xi'an University of Architecture and Technology. The experimental equipment was a computer-controlled electro-hydraulic servo rock mechanics testing machine (shown in Fig. 2) developed by Xi'an Lichuang Instrument and Equipment Co., Ltd, which can provide sine-waves for cyclic loading and unloading. Its maximum loading intensity was 600 kN, and the disturbance frequency was 0~3 Hz. This study mainly conducted the uniaxial compression test and cyclic loading and unloading test, with the loading method of stress control. The initial preloading stress was 0.30 kN, and ensured that the rock was in contact with the indenter of mechanical testing machine.

The uniaxial compression test results as shown in Fig. 3 of the same batch specimens show that the stress-strain curve has undergone four stages of compression compaction stage (*oa* stage), elastic deformation stage (*ab* stage), damage deformation stage (*bc* stage), and instability rupture stage (*cd* stage). The stress-strain curve drops rapidly after reaching peak strain, showing a brittle failure characteristics. The uniaxial compressive strengths of rock samples HR-1~HR-3 are 74.56 MPa, 76.53 MPa, and 78.01 MPa, respectively, and the corresponding average strength is 76.37 MPa. The experimental results (Karma and

Lobkovsky 2004) confirmed that the prefabricated rock samples with typical brittle fracture characteristics belong to hard rock.

According to the uniaxial compression test results, initial upper limit stress of cyclic loading and unloading tests was set as 15 MPa, which was 19.64% of the average uniaxial compressive strength (76.37 MPa), and the lower limit stress ($\Delta\sigma_0$) in each cycle was 5 MPa, and then reloading until it exceeded the maximum axial stress of the upper stage by 5 MPa (stress increament $\Delta\sigma$). The maximum axial stresses (upper limit stress) were 0, 15, 5, 20, 5, 25, ... , 50, 5 MPa, ..., until the hard rock was destroyed. This test mainly refers to the Rock Code for Hydropower and Water Conservancy Engineering (DLT53682007) (Li, 1995). The cyclic loading and unloading tests were carried out on the hard rocks HR-4, HR-5, HR-6, and HR-8 with the loading and unloading rates of 0.10, 0.25, 0.40, and 0.55 MPa/s, respectively. Fig.4 shows the stress loading and unloading path.

3. Experimental results and analysis

3.1 Morphological characteristics of stress - strain curves

The stress-strain curves morphology at different loading and unloading rates are shown in Fig. 5. It can be seen from Fig. 5 that the stress-strain curves are similar in distribution shapes. After compressive compaction, elastic deformation and plastic deformation, they gradually transition into the cyclic deformation stage, and typical brittle failure (Davies and Hunter 1963; Zhou *et al.* 2020) occurs after several cyclics. The direct effects of loading and unloading rate on stress-strain curve are mainly reflected in the density degree of hysteretic loops and strength deterioration. With increasing loading and unloading rate, hysteretic loops of stress-strain curve generally change from sparse distribution to dense distribution, showing that the loading-unloading effect intensifies the initiation, expansion speed and damage accumulation of internal cracks.

Compared with soft rock, hysteresis loop of hard rock in this study at the same loading and unloading rate does not appear sparse-dense-sparse distribution characteristics (Zhou *et al.* 2020), but presents a dense-sparse distribution characteristics. The analysis believes that the hard rock has homogeneous and low porosity characteristics, and its initial upper limit stress of preloading before unloading will compact the partial pores, and rock stiffness is relatively improved. The cyclic stress amplitude in the early stage is small (5~35 MPa), and the maximum upper limit stress is only 45.83% of its uniaxial compressive strength, which is obviously less than the damage threshold (Taheri *et al.* 2020; Sun 2021). The mainly elastic deformation does not cause fatigue damage at this time, and the increment in residual strain is not significant, and the hysteresis loops are densely distributed in the early loading and unloading stage. With increasing the upper limit stress (greater than 35 MPa), hard rock begins to change from elastic deformation to excessive plastic deformation, its internal cracks gradually sprout, the accumulated fatigue damage increases,

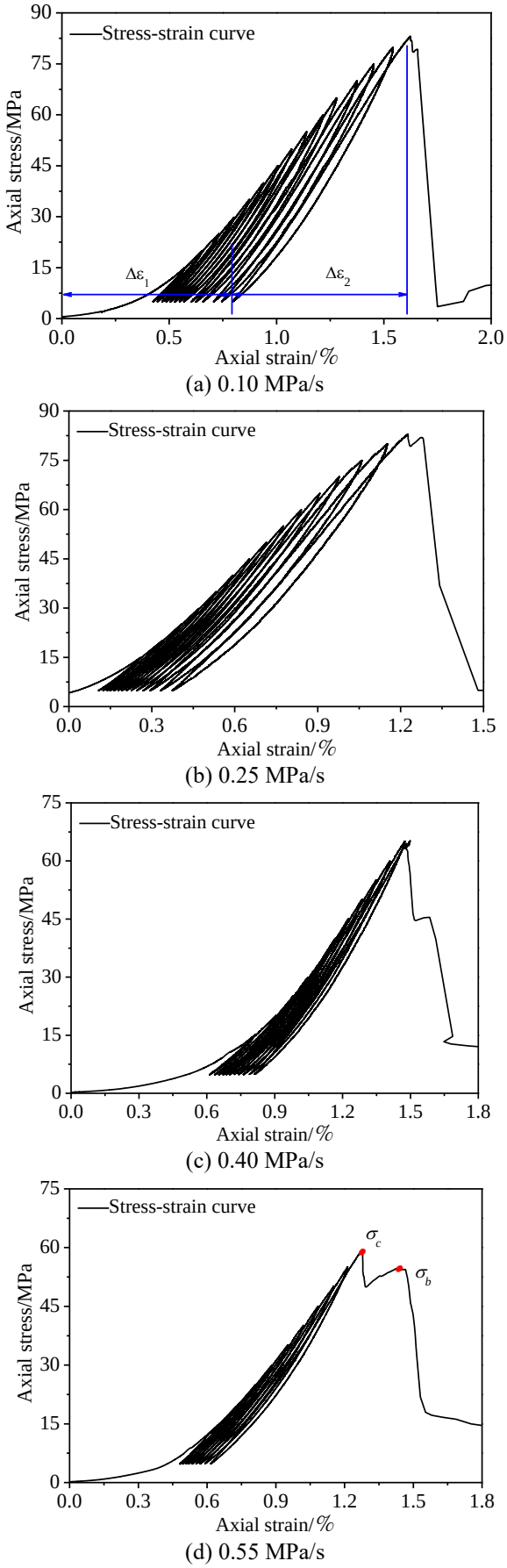

Fig. 5 Stress-strain curves at different loading and unloading rates

the residual deformation increases sharply and the area of hysteresis loop increases simultaneously, and this then leads to a sparse distribution of the hysteresis loop.

The rock exhibits dynamic strain characteristics during the loading and unloading process, the strain variables that can be recovered are called elastic strain that cannot be recovered are called residual strain. Fatigue life represents the maximum number of loading and unloading cycles that a rock can withstand before it ruptures. Fig. 6 shows the relationships between residual strain, elastic strain, fatigue life and loading and unloading rate, and the value ranges of residual strain and elastic strain are shown in Fig. 6(a). It is seen from Fig. 6(a) that when the loading and unloading rate increases from 0.10 to 0.55 MPa/s, residual strain and elastic strain are decreased by 64.05% and 24.97%, respectively. According to Fig. 6(b) shows that the loading and unloading rate has a deterioration effect on the fatigue life. When the loading and unloading rate is 0.10~0.25 MPa/s, hard rocks HR-4 and HR-5 complete 14 cycles and fatigue rupture occur in the 15th loading section. When the loading and unloading rate is 0.40~0.55 MPa/s, only 11 and 9 complete cycles of hard rocks HR-6 and HR-8 are broken, and the average cycle is reduced by 28.57%. This indicates that with the increase of cycle number, a large number of irreversible deformation accumulated in hard rock aggravates the cyclic weakening effect of fatigue deformation. The regression analysis shows that the residual strain, elastic strain and fatigue life decay linearly with increasing loading and unloading rate.

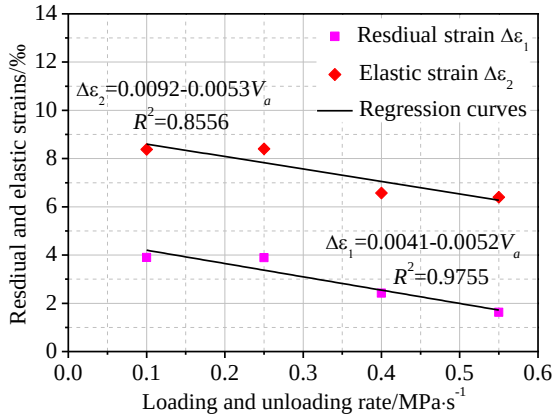

(a) Residual strain and elastic strain

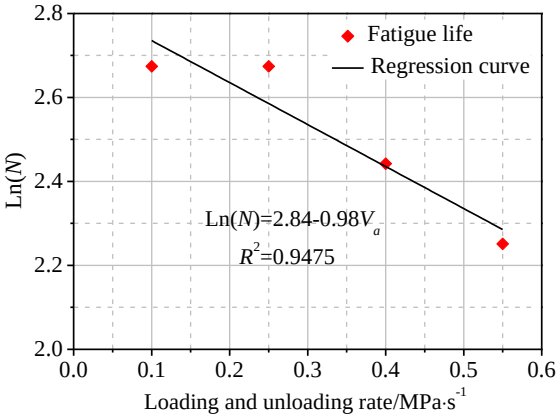

(b) Fatigue life

Fig. 6 Relationships between residual strain, elastic strain, fatigue life and loading and unloading rate

3.2 Strength characteristics under cyclic loading and unloading

It has been shown in Fig. 5 that the envelope line of stress-strain curve is distributed in a lower concave shape and then reaches its peak strength after compression compaction, elastic deformation and plastic deformation stages. The stress-strain curve decreases by 1.16~31.07% after passing the maximum bearing capacity (σ_c as shown in Fig. 5(d)), but the hard rock still has a certain bearing strength. With increasing loading time, axial stress rises and reaches the second peak strength (σ_b as shown in Fig. 5(d)), indicating that the hard rock still has potential bearing capacity despite the formation of macroscopic fractures but no macroscopic slip plane. This is due to the superimposed effect (Hooker *et al.* 2019) of pores collapse and cracks closure during fracture process, and this failure mode is called stable fracture type. When the bearing strength crosses the second peak strength, its stress-strain curve falls rapidly, and the hard rock produces transient rupture. It is seen that the second peak strength indicates the occurrence of complete brittle failure, which can be called the brittle strength (σ_b) and the corresponding strain is called the brittle strain in this study.

3.2.1 Peak strength characteristic

To further study the influence characteristics of loading and unloading rate on the peak strength of rock under cyclic loading and unloading, corresponding relationship between peak strength and loading and unloading rate is given based on Fig. 5, as shown in Fig. 7.

As can be seen from Fig. 7(a) that the peak strength increases first and then decreases with the loading and unloading rate increases, which is consistent with the existing experimental results (Taheri *et al.* 2020). When the loading and unloading rate increases from 0.10 to 0.25 MPa/s, peak strength increases from 82.52 to 83.26 MPa; when the loading and unloading rate increases from 0.40 to 0.55 MPa/s, peak strength decreases from 65.15 to 59.56 MPa. Compared with the average uniaxial compressive strength (76.37 MPa), the acceleration effect (Zhou *et al.* 2020) is observed at the loading and unloading rates of 0.10~0.25 MPa/s, and its peak strength is increased by 8.05%~9.02%, but the strengthening effect is negatively correlated with the loading and unloading rate. However, when the loading and unloading rate increases from 0.40 to 0.55 MPa/s, the hard rock has a significant deterioration effect and its peak strength decreases by 14.69%~22.01%.

The above analysis shows that the small expansion of internal microcracks at relatively low loading and unloading rates results in the less accumulated damage, and the peak strength exhibits an acceleration effect. However, with increasing loading and unloading rate, the violent cyclic disturbance effect induces new cracks to sprout and expand quickly, aggravating the expansion and penetration of original cracks and new cracks, causing the structural adjustment and stress redistribution of rock skeleton, leading to the accumulation of irreversible deformation,

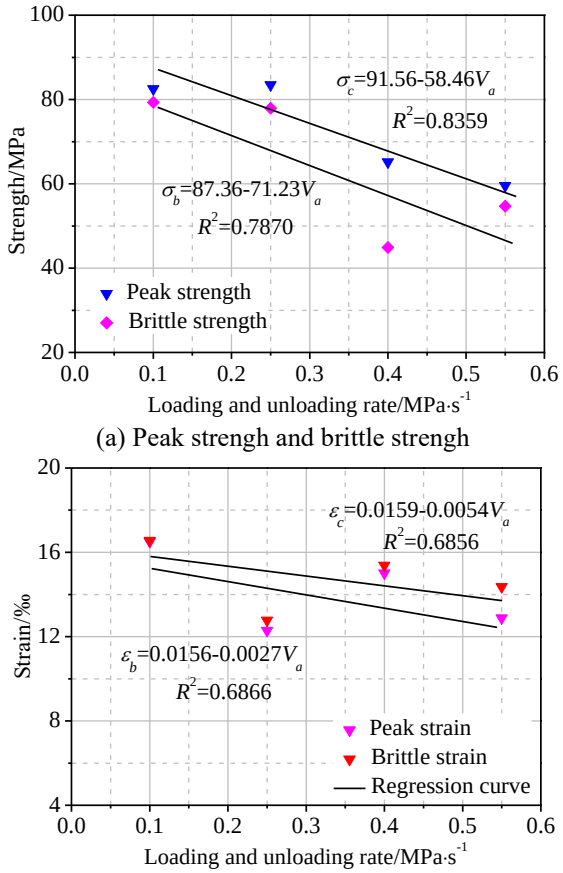

(a) Peak strengh and brittle strengh

(b) Peak strain and brittle strain

Fig. 7 Strength and strain characteristics at different loading and unloading rates

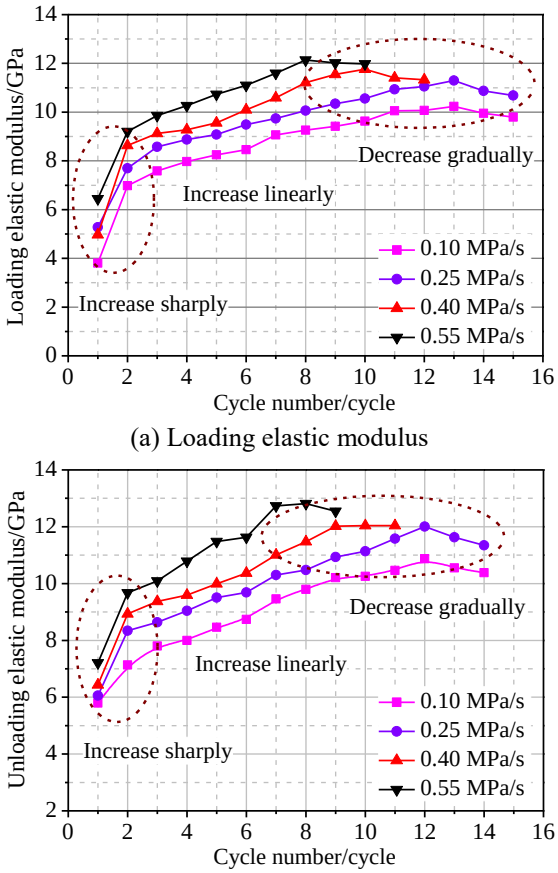

(a) Loading elastic modulus

(b) Unloading elastic modulus

Fig. 8 Elastic modulus at different loading and unloading rates

significantly improving the damage degree, and thus deteriorating the peak strength. In addition, compared with the natural rock, the physical characteristics of the hard rock poured in the laboratory are discrete. It is easy to cause stress concentration phenomenon when the quartz sand is encased in cement and crystals of uneven strength are formed, and its stress concentration level is generally positively related to loading and unloading rate, which further aggravates the strength deterioration.

3.2.2 Brittle strength characteristics

The corresponding relationship between brittle strength and loading and unloading rate is given based on Fig. 5, as shown in Fig. 7(a). It can be seen from Fig. 7(a) that the brittle strength at the same loading and unloading rate is always less than peak strength. Except for the abnormal brittle strength of hard rock HR-6, brittle strength of other rocks generally decrease linearly with increasing loading and unloading rate. When the loading and unloading rate increases from 0.10 to 0.55 MPa/s, the brittle strength decreases by 31.03%. Compared with the soft rock, the hard rock has significant brittle deformation characteristic, and the unloading deformation is usually more obvious than loading deformation (Komoroczi *et al.* 2013), and more irreversible deformation will be accumulated per unit time. Therefore, the weakening effect of loading and unloading effect on the potential bearing capacity of rock skeleton is more severe.

Compared with the conventional uniaxial loading tests as shown in Fig. 3, brittle strengths at the loading and unloading rate of 0.10~0.25 MPa/s are approximately equal to the average uniaxial compressive strength (76.37 MPa), while the brittle strengths at the loading and unloading rate of 0.40~0.55 MPa/s are reduced by 28.38%~41.19%, and its strength deterioration is obviously increased. The peak strain and brittle strain corresponding to peak strength and brittle strength are shown in Fig. 7(b). Similar to the change characteristics of peak strength and brittle strength, the peak strain and brittle strain also generally show a linear decay trend with increasing loading and unloading rate.

3.3 Characteristics of elastic modulus under cyclic loading and unloading

3.3.1 Loading elastic modulus

Linear fitting of the data (50%σ_c ± 5 MPa) in the elastic deformation phase of loading and unloading stress-strain curves, corresponding linear slopes are the loading elastic modulus and unloading elastic modulus as shown in Fig. 8(a). The loading and unloading rates have a significant influence on the variation character of loading elastic modulus, the higher the loading and unloading rate is, the greater the loading elastic modulus. With increasing cycle number, loading elastic modulus firstly increases sharply, then increases linearly, and finally decreases gradually. The

boundary points of the three stages are significantly related to the loading and unloading rates.

The variation characteristics of elastic modulus in the loading and unloading process can reflect the damage degree inside the hard rock. The evolution characteristics of loading elastic modulus are summarized as follows:

When the stress ratio (σ/σ_c) of selected axial loading stress to uniaxial compressive strength is less than 17.29%, the early loading stress has an obvious strengthening effect on hard rock, and loading elastic modulus increases sharply with increasing cycle number. This is because the internal primary cracks are gradually compressed and closed, which improves the stiffness of hard rock. In this stage, loading elastic modulus is 3.80~9.21 GPa with a growth rate of 42.80%~83.22%.

When the stress ratio σ/σ_c is greater than 17.29% and less than 57.62%~86.43%, the cyclic disturbance effect and increased upper limit stress induce the new cracks begin to sprout, the fatigue damage caused by the crack expansion gradually offset the early strengthening effect, and the increasing trend of loading elastic modulus is gradually slowed down, and then shows an approximate linear growth, the greater the loading and unloading rate, the faster the growth rate of loading elastic modulus.

When the stress ratio σ/σ_c is more than 57.62%~86.43%, the continuously increased upper limit stress induces the expansion of internal microcracks and gradually occupies the dominant advantage, the primary and secondary cracks begin to intersect and form macroscopic cracks, thus leading to a gradual reduction of loading elastic modulus, which coincides with the evolution characteristics of loading elastic modulus of chlorite phyllite and sandstone (Sun *et al.* 2021). This is because the cyclic loading and unloading disturbance leads to the slip of crystal particles, adjustment of rock skeleton structure and stress rearrangement (Bahrani *et al.* 2016), resulting in the increased irreversible deformation and damage degree, thus leading to a gentle or even reduction of loading elastic modulus.

3.3.2 Unloading elastic modulus

Compared with the variation characteristics of loading elastic modulus, unloading elastic modulus experiences a three similar evolutionary stages of a sharp increase, then linear increase and finally gradual decrease with increasing the cyclic number, as shown in Fig. 8(b). The stress boundary point of axial stress is the same as that in Fig. 8(a). Compared with the evolution trend of loading elastic modulus and unloading elastic modulus at the initial stage of cyclic loading and unloading, the unloading elastic modulus (5.80~7.21 GPa) is much larger than that of loading elastic modulus (3.81~6.44 GPa), and the former is about 1.12~1.52 times of the latter. The elastic modulus curves of loading and unloading approach gradually as the upper limit stress increases, indicating that the two elastic modulus are approximately equal and the hard rock is approximately a completely brittle material (Liyanage *et al.* 2013). As the upper limit stress continues to increase, the elastic modulus curves of loading and unloading gradually separate with the cycle numbers increases, which means that the primary cracks and secondary pores begin to extend and even connect, and the cumulative damage continues to increase, thus leading to the decrease of loading elastic modulus.

According to the relation curves between elastic modulus at different loading and unloading rates, it can be seen that the evolution stage of elastic modulus under loading and unloading conditions are similar. The numerical regression analysis shows that the elastic modulus of loading and unloading has a first-order exponential function relationship with cycle number, and the regression equation can be expressed as follows:

$$E = E_0 \operatorname{Exp}(-\frac{N}{t}) + Y \tag{1}$$

where E is the elastic modulus of loading and unloading (GPa); E_0 is the response strength of elastic modulus (GPa); N is the cycle number (cycle); $1/t$ is the evolution coefficient of elastic modulus with the cycle number (cycle^{-1}); Y is regression coefficient of elastic modulus (GPa); The parameters E_0, t, Y are linear with the loading and unloading rate (V_a):

In loading process: E_0=-1.44V_a-7.39 (R^2=0.9356), t_1=-1.35V_a+3.20 (R^2=0.8966), Y=4.64V_a+9.61(R^2=0.9527);

In unloading process: E_0=-3.30V_a-5.91 (R^2=0.9563), t_1=-5.45V_a+6.30 (R^2=0.8663), Y=4.22V_a+10.91 (R^2=0.9768).

3.4 Critical damage factor

The above analysis shows that the loading and unloading rate have significant effects on mechanical parameters such as peak strength and elastic modulus, and the damage and deformation are caused by the circular disturbance effect in essence. The closure of primary cracks is accompanied by the initiation and expansion of new cracks in loading stage, and the adjustment of skeleton structure and stress redistribution in unloading stage aggravate the generation of irreversible deformation. The damage is essentially an excessive process of plastic deformation to the ultimate bearing point or peak strength, which is accompanied by the accumulated damage caused by irreversible deformation, so the peak strain point during the rock sample damage corresponds to critical damage factor.

If the rock sample is regarded as an isotropic continuous medium, the corresponding relationship between effective stress and damage factor can be obtained according to the Lemaitre strain equivalence principle (Stevens and Holcomb 1980, Lemaitre 1984).

$$\sigma = E\varepsilon(1-D) \tag{2}$$

where σ is the effective stress (MPa); E is the elastic modulus (GPa); ε is the axial strain; D is the damage factor, D=0 means no damage, D=1 means the rock failure.

Due to the strength and strain characteristics of rock sample follow the Weibull distribution, rock damage factor can also be considered to follow the Weibull distribution, and the damage factor can also be described by the density function of the Weibull statistical distribution function. Therefore, the peak intensity corresponds to the critical damage factor.

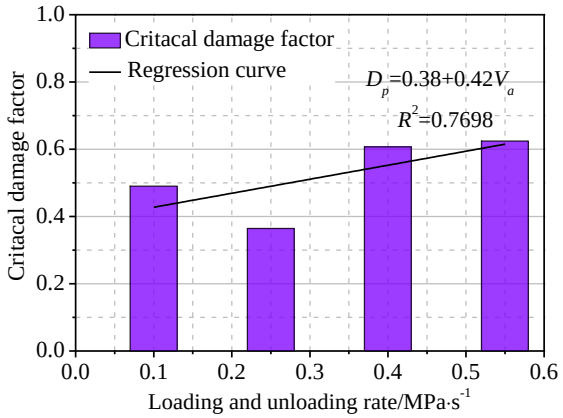

Fig. 9 Critical damage factor at different loading and unloading rates

$$D_p = 1 - \frac{\sigma_p}{E\varepsilon_p} \tag{3}$$

where σ_p is the peak stress (MPa); ε is peak strain; D_p is critical damage factor.

It is seen from the Eq. (3) that the critical damage factor during rock rupture is related to the peak stress, elastic modulus and peak strain, which can be obtained from the data in Figs. 7~8. Since this paper mainly studies the influence characteristics of loading and unloading rates on critical damage factor, the peak stress, elastic modulus and peak strain are taken from the stress-strain curve of the last loading stage. The relationship between critical damage factor and loading and unloading rates is shown in Fig. 9.

Fig. 9 shows that the critical damage factor generally increases as the loading and unloading rate increases. The critical damage factor of hard rock HR-5 is 0.36, which is obviously lower than hard rock HR-4. This is because the axial loading has a strengthening effect on the strength when the loading and unloading rate is less than 0.25 MPa/s, and the evolution degree of fracture initiation and propagation is lower than 0.10 MPa/s. When the loading and unloading rate increases to 0.40 and 0.55 MPa/s, the critical damage factor are 0.60 and 0.63, increasing 64.25% and 72.99% compared to hard rock HR-5, respectively. It can be seen that with increasing loading and unloading rate, the cracks expansion becomes more intense, the penetration degree and expansion phenomenon of cracks become more significant, the accumulated fatigue damage gradually increases and deterioration degree is aggravated. Regression analysis shows that the critical damage factor has an approximately linear relationship with increasng loading and unloading rate.

3.5 Macroscopic failure mode and fractal characteristics

3.5.1 Macroscopic failure mode analysis

The macroscopic fracture characteristics at different loading and unloading rates are shown in Fig. 10. It can be seen that the macroscopic failure modes mainly include oblique shear through failure and tensile through failure, containing at least one oblique or longitudinal through fractures, and the fracture number and failure degree on the rock surface are related to the loading and unloading rate.

Fig. 10 shows that the hard rock have fewer macroscopic cracks and low penetration level at relatively low loading and unloading rates (0.10~0.25 MPa/s), but a relatively obvious slip surface is formed and mainly undergoes shear failure. The upper part of hard rock HR-4 forms an obvious wedge-shaped fracture area due to the end constraint, then induces the wedge-shaped rock to invade the lower rock and occurs the phenomenon of cross-bedding, and two oblique shear cracks intersect to form a tensile fracture and gradually connecte to the rock bottom. The oblique shear crack is formed in the lower part of hard rock HR-5, leading to the formation of split rock strips at the 1/4 position on the right. The main crack penetrates downward gradually, resulting in a tensile crack at the lower end of rock. Compared with hard rock HR-4, the cracks number and penetration degree of hard rock HR-5 are significantly increased. In addition, there are rock pieces shoot off, peeling and breaking phenomena, and powdery rock foam appears on the oblique shear fracture surface on the surface of hard rocks HR-4 and HR-5. This is due to the particle dislocation and sliding effect caused by the loading and unloading action that aggravate the friction between mineral particle structures.

At relatively high loading and unloading rates (0.40~0.55 MPa/s), the rocks are dominated by tensile failure, the shear crack decrease and tensile crack increase significantly. The tensile crack and oblique shear crack in the upper part of hard rock HR-6 first spread through, leading to the tensile cracks in the upper right rock block. The stress imbalance on the right side causes the rock to tilt to the left and macroscopic fracture occurs, and the newly formed longitudinal strip rock block appears fracture. With increasing loading and unloading rate, the upper part of hard rock HR-8 is broken explosively (Mlakar *et al.* 1993) due to rapid tension, forming a longitudinal fracture network with a significant degree of fragmentation. As the upper limit stress continues to be loaded, the upper penetrating cracks extend downward and gradually form a macro crack, and the rock surface is accompanied by fragments ejected to form a missing area.

Fig. 11 shows the distribution patterns of macroscopic rupture fragments at different loading and unloading rates.

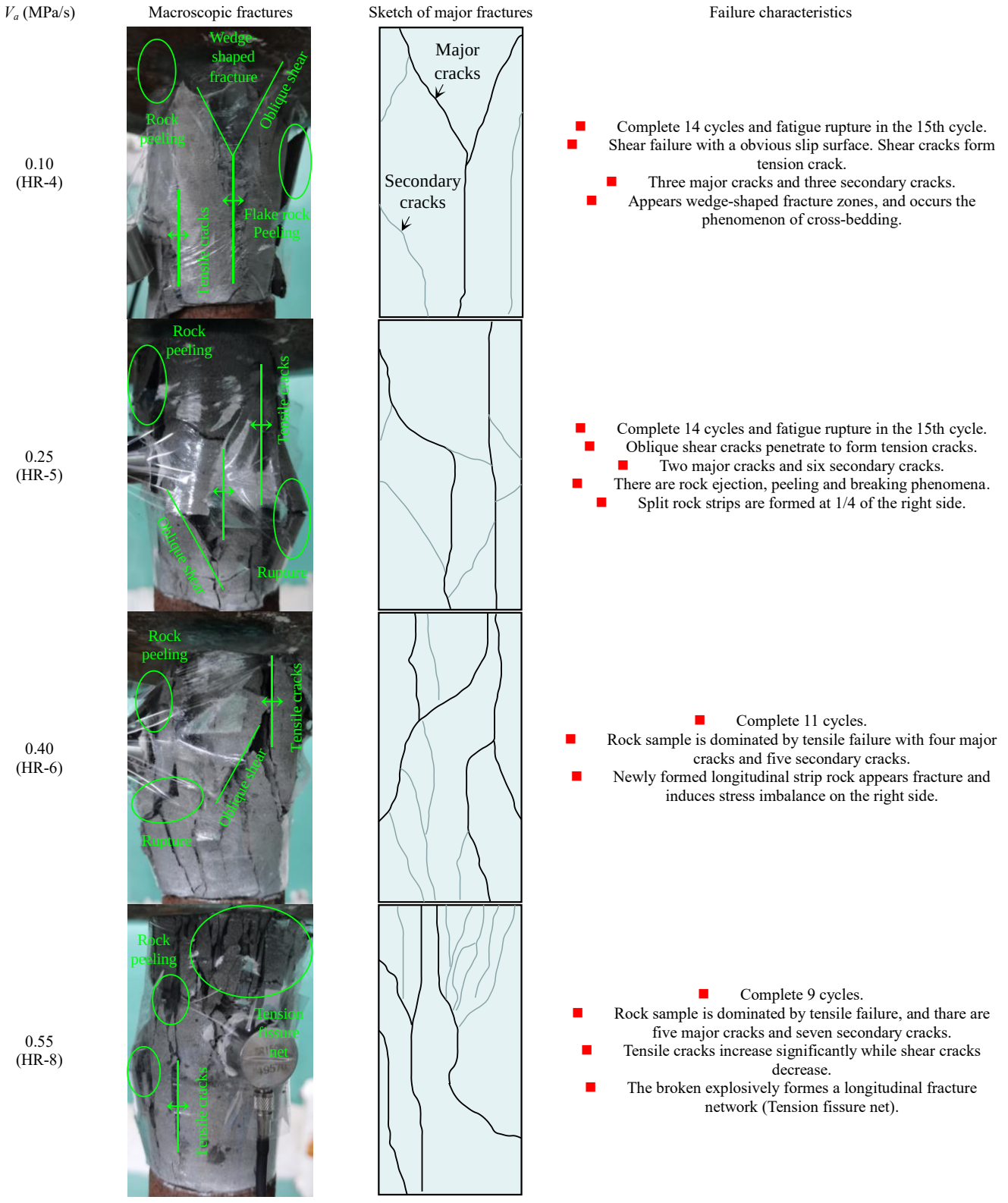

Fig. 10 Macroscopic fracture characteristics

As the rock samples are wrapped with plastic wrap to prevent the fragments from scattering, there is some color difference between the rocks and fragments. Fig. 11 shows that the failure mode gradually shifts from oblique shear failure to tensile failure with the increase of loading and unloading rate. The number of macroscopic cracks on rock surface, penetration degree of cracks, and rupture area increase significantly, while the fragments number increase, fragments size decrease and uniformity is obviously better. It can be seen that the increase of loading and unloading rate aggravates the fragmentation degree, which is consistent with the existing literature (Karma *et al.* 2004).

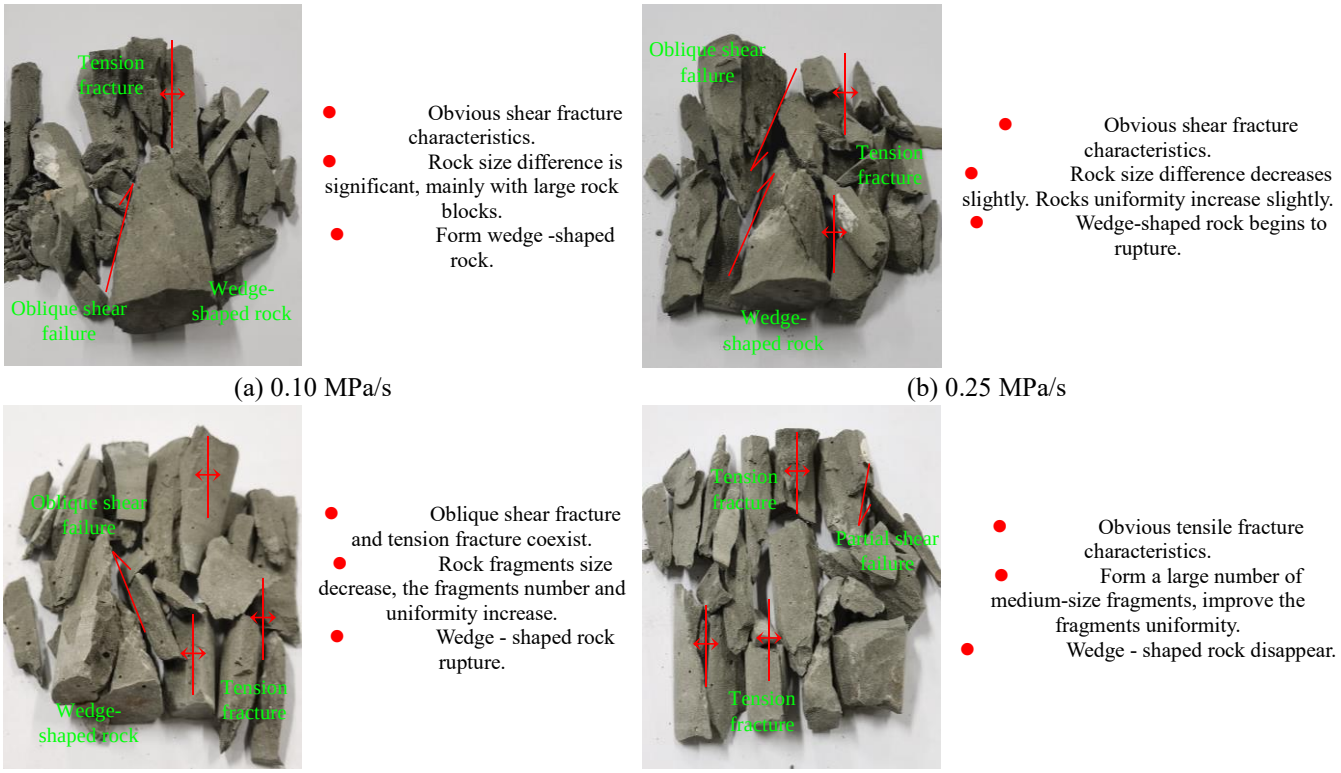

Fig. 11 Distribution patterns of rock fragments

Table 1 Distribution interval and weight percentage of rock fragments

Distribution interval (mm)	Weight /g and weight percentage /%			
	0.10 MPa/s	0.25 MPa/s	0.40 MPa/s	0.55 MPa/s
0~0.63	1.31/0.34	1.49/0.38	2.06/0.53	2.52/0.63
0.63~1.25	2.12/0.55	1.48/0.37	3.49/0.90	3.16/0.79
1.25~2.50	4.50/1.16	3.61/0.91	2.99/0.77	3.22/0.81
2.50~5	10.02/2.58	10.20/2.57	10.06/2.59	10.06/2.52
5~10	20.11/5.18	30.02/7.57	40.01/10.30	60.02/15.05
10~20	80.06/20.64	90.11/22.72	130.11/33.48	80.11/20.09
20~40	150.04/38.68	260.10/65.58	200.02/51.47	240.00/60.20
40~50	120.12/30.97	-	-	-

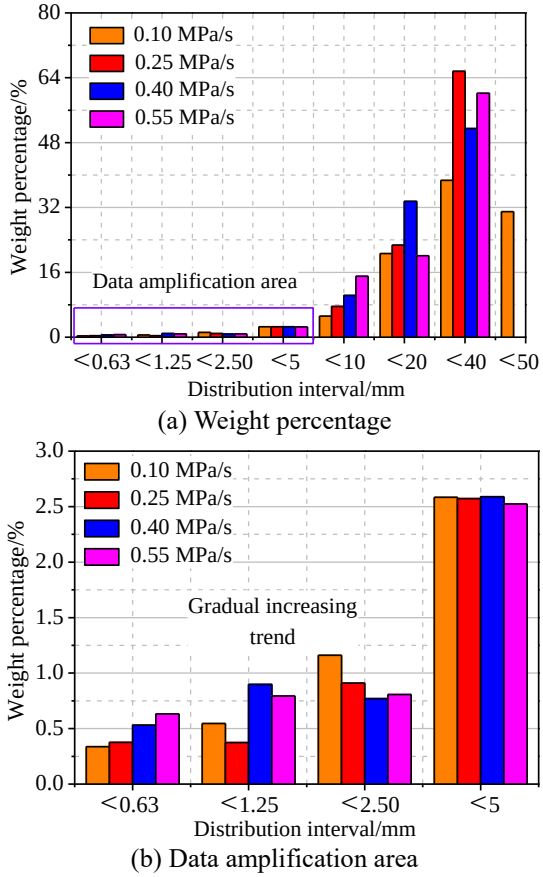

Fig. 12 Weight percentage of rock fragments

Moreover, the typical wedge-shaped fracture areas are formed at the end position of hard rocks HR-4 and HR-5, and the wedge-shaped fractures of hard rock HR-6 are tension-broken, and no wedge-shaped fractures appear at hard rock HR-8. It can be seen that the increase of loading and unloading rate reduces the end constraint effect, and makes the rocks more prone to tensile fracture. However, there is no strict correspondence between failure mode and axial peak strength.

3.5.2 Distribution characteristics of fragments weight

Fig. 11 indicates that the fragments size and weight distribution characteristics of broken fragments show a certain fractal law. To reasonably analyze the distribution characteristics of fragment weight, sieving and weighing the broken fragments with the standard screens with diameters (characteristic dimension r) of 0.63, 1.25, 2.50, 50, 5.00, 10,

20 and 40 mm. The rock fragments are divided into 8 grades including 0~0.63, 0.63~1.25, 1.25~2.50, 2.50~5, 5~10, 10~20, 20~40. The distribution interval and weight percentage of rock fragments at different loading and unloading rates are shown in Table 1, "-" indicates that there is no rock fragments of corresponding size in this distribution interval. The numbers before and after the "/" are weight and weight percentage, respectively.

Fig. 12 shows the weight percentage of rock fragments at different loading and unloading rates. It can be seen that the loading and unloading effect has a significant impact on the fragments distribution, mainly reflect in the fragmentation degree and fragments uniformity, the greater the loading and unloading rate, the more obvious the fragmentation degree, the more significant the fragments uniformity. When the loading and unloading rate increases from 0.10 to 0.55 MPa/s, the fragments weight within 0~2.50 mm is less than 5 g and weight percentage is less than 2%. Although the weight percentages within the same distribution interval increase slightly with the loading and unloading rate, its increasemen is not significant. It is thus shown that the loading and unloading rate has little impact on the weight percentage distribution of small-size fragments (0~2.50 mm).

The following conclusions can be summarized from Fig. 12. ① Compared to the fragment weight within 0~2.50 mm, the fragment weight within 2.50~5 mm is greater than 10 g, its weight percentage is 2.52%~2.59%, and the corresponding increase range is greater than 30%. ② The fragments weight percentage within 5~20 mm generally increase with the loading and unloading rate. It is shown that the number of medium-size fragments (2.50~20 mm) increases significantly with the loading and unloading rate, and the fragments uniformity is significantly improved, which is consistent with the previous analysis. ③ For the fragments within 20~50 mm, the fragment sizes larger than 40 mm appear at 0.10 MPa/s, while the fragment sizes at 0.25~0.55 MPa/s is mainly concentrated on 20~40 mm. The weight percentages within 20~50 mm are 69.65%, 65.58%, 51.47%, and 60.20%, respectively, it generally shows a decay trend with increasing loading and unloading rate. This implies that the loading and unloading effect reduces the number of large-size fragments (20~50 mm) and increases the number of medium-size fragments, and thus improving the fragments uniformity.

In addition, Fig. 12 also shows that ① when the fragments size is less then 5 mm, the difference in weight percentage within the same distribution interval gradually decreases, and the difference within 2.50~5 mm is the smallest; ② when the fragments size is more then 5 mm, the weight percentage and its difference correlation in the same distribution interval gradually increase again, which is the same as the macroscopic failure mechanism. Figs. 11~12 show that the larger the loading and unloading rate, the large-size fragments is significantly reduced and the fragment weight decreases accordingly, and the larger weight fragments transform to smaller weight fragments. Therefore, the higher the loading and unloading rate within a certain range, the greater the possibility of dynamic fracture.

3.6 Fractal characteristics of rock fragments

Fractal theory (Outer *et al.* 1995) is widely applied in rock mechanics to study the fractal characteristics and statistical relationship between fragments distribution and particle size. In this test, the weight distribution law is obtained by screening-weighting method, and then the distribution function of fragments size is as follows:

$$Y = \frac{M(r)}{M_T} = r^{3\text{-}D_r} \tag{4}$$

where r is the characteristic size of statistical interval of fragments (mm); $M(r)$ is the fragments weight whose equivalent particle size (R) is less than characteristic size (r) (g); M_T is the total weight of rock fragments; $M(r)/M_T$ is the cumulative weight percentage of fragments with equivalent particle size less than characteristic size (r); D_r is the fractal dimension.

The rock fragmentation process shows a self-similarity characteristic, and there is an equivalent relationship between equivalent diameter (R) and equivalent volume of rock fragments.

$$R = \sqrt[3]{V} = \sqrt[3]{ldh} \tag{5}$$

where V is the equivalent volume of rock fragments; l, d and h are the equivalent length, equivalent width and equivalent height, respectively.

Take the natural logarithm of both sides of Eq. (4) to get:

$$Ln[\frac{M(r)}{M_T}] = (3 - D_r)Lnr \tag{6}$$

According to Eq. (6), $Ln[M(r)/M_T] \sim Lnr$ has a linear relationship, and 3-D_r is the linear slope in log-coordinates $Ln[M(r)/M_T] \sim Lnr$. The distribution relationship between fragments weight and particle size can be obtained based on Fig. 12, and then the numerical regression can determine the fractal dimension of rock fragments. Fig. 13 shows the $Ln[M(r)/M_T] \sim Lnr$ curve of rock fragments at different loading and unloading rates. It can be seen that the fragments weight is linearly correlated with the characteristic size (r). The fractal dimension can be used to quantitatively characterize the degree of rock fragments. With increasing loading and unloading rate, fractal dimension of rock fragments showes an increasing trend of 1.56, 1.67, 1.78, 1.81, respectively. It can be seen that the loading and unloading rate reduces the large - size fragments, and the large - size fragments are gradually transformed into medium-size fragments.

Fig. 14 shows the relationship between fractal dimensions (D_r) and loading and unloading rate (V_a), which grows nonlinear with increasing loading and unloading rate. When the loading and unloading rate changes from 0.10 MPa/s to 0.25 MPa/s, fractal dimension increases from 1.56 to 1.67 with an increase of 7.05%; when the loading and unloading rate changes from 0.40 MPa/s to 0.55 MPa/s,

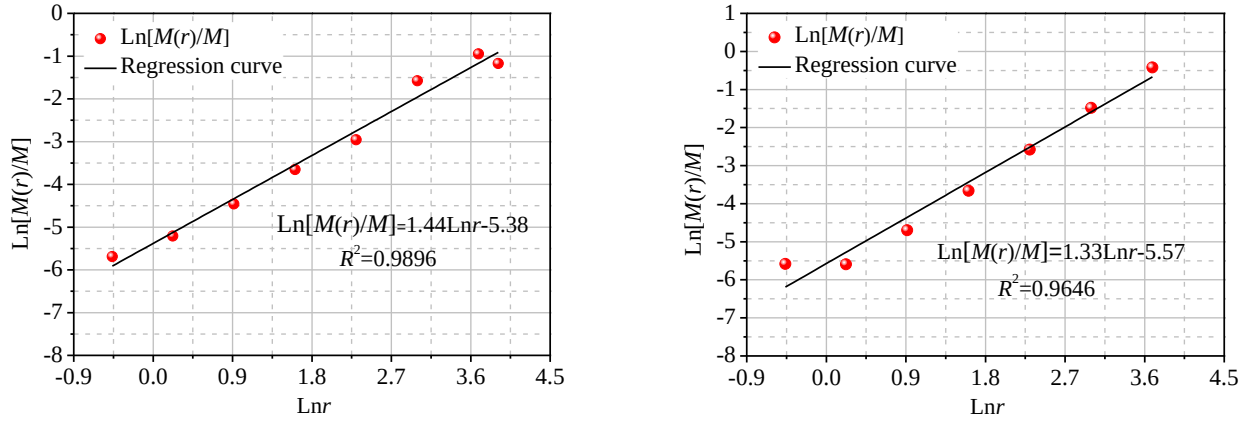

Fig. 13 Logarithmic curves of fragments weight and characteristic size

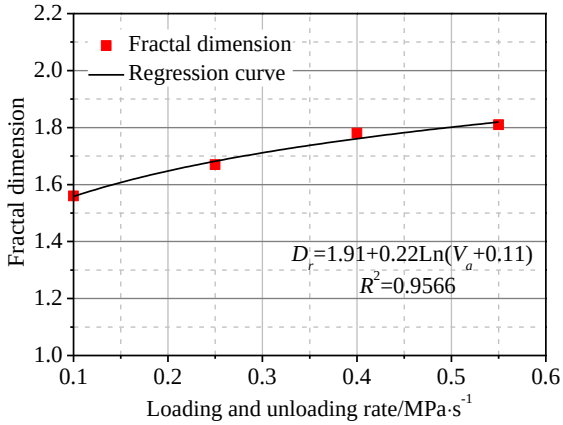

Fig. 14 Relationship between fractal dimension and loading and unloading rate

fractal dimension increases from 1.78 to 1.81 with an increase of 1.69%, and its growth rate tends to slow down. Data regression shows that the fractal dimension of rock fragments is logarithmic function related to the loading and unloading rate. It can be seen that the larger the loading and unloading rate, the larger the fractal dimension and the higher the fragmentation degree, and the better the fragmentation uniformity. This is because the rock deformation under the cyclic loading and unloading path exhibits a loading-unloading cyclic effect, and the disturbance mechanism is relatively complicated. The internal structure of rock has an interactive stress response to loading and unloading effect, and the stress coordination and damage accumulation are more adequate, which in turn leads to the hard rock being more prone to fracture and instability.

3.7 Discussion

Fig. 7(a) shows that the peak strength increases first and then decreases with the loading and unloading rate increases, and there is no acceleration effect. This is due to the more complex stress path of cyclic loading and unloading test compared with conventional uniaxial compression test, the loading and unloading rate exhibits a stepwise control effect. The loading and unloading rate in different stages has different activation sensitivity to the degree of crack opening, which in turn causes the strengthening and weakening characteristics of peak strength. In addition, the cemented body of different strength is formed by cement wrapping quartz sand in the artificially poured rock samples, which aggravates the stress concentration inside the rock and increases the possibility of strength deterioration.

Based on the analysis of the viscosity, inertial effect and thermal activation effect of rock materials, the peak strength of rock sample usually increases or gently changes with the increase of strain rate or loading rate, while the acceleration

effect is often affected by lithology, strain effect and stress distribution characteristics inside the rock. Qi *et al.* (2019) established the competing theory of thermal activation mechanism and macroscopic viscosity mechanism, which indicated that the loading rate played a different leading role at different strain rate stages. With the loading rate increases, the strength of hard rocks such as limestone, granite, and basalt does not increase accordingly, but the acceleration effect appears only when the loading rate is in a particular state such as quasi-static loading. Li *et al.* (2016) also found that the peak strength and residual strength of coal rock both increase at first and then decrease with increasing loading rate. Zhou *et al.* (2020) showed that chlorite phyllite exhibited a certain strength weakening characteristics under cyclic conditions. It can be seen that the evolutionary character of peak strength under cyclic loading and unloading action is not completely uniform. The cyclic disturbance of high loading and unloading rate or high strain loading and unloading condition on rock is extremely severe, and then the strength weakening phenomenon appears, which is related to the control mode of cyclic loading and unloading, load increment, lithology and stress state.

4. Conclusions

Fig. 14 shows the relationship between fractal dimensions (D_r) and loading and unloading rate (V_a), which grows nonlinear with increasing loading and unloading rate. When the loading and unloading rate changes from 0.10 MPa/s to 0.25 MPa/s, fractal dimension increases from 1.56 to 1.67 with an increase of 7.05%; when the loading and unloading rate changes from 0.40 MPa/s to 0.55 MPa/s, fractal dimension increases from 1.78 to 1.81 with an increase of 1.69%, and its growth rate tends to slow down. Data regression shows that the fractal dimension of rock fragments is logarithmic function related to the loading and unloading rate. It can be seen that the larger the loading and unloading rate, the larger the fractal dimension and the higher the fragmentation degree, and the better the fragmentation uniformity. This is because the rock deformation under the cyclic loading and unloading path exhibits a loading-unloading cyclic effect, and the disturbance mechanism is relatively complicated. The internal structure of rock has an interactive stress response to loading and unloading effect, and the stress coordination and damage accumulation are more adequate, which in turn leads to the hard rock being more prone to fracture and instability.

Acknowledgments

The present work was supported by the National Natural Science Foundation of China (No. 5217080601, 51578447), the Science and Technology Innovation Team of Shaanxi Innovation Capability Support Plan (No. 2020TD005), and Shaanxi Province Housing and Rural Construction Science and Technology Plan (No. 2019-K39). The financial supports are gratefully acknowledged and the data are available for the journal.

References

Bahaaddini, M., Sharrock, G. and Hebblewhite, B.K. (2013), "Numerical investigation of the effect of joint geometrical parameters on the mechanical properties of a non-persistent jointed rock mass under uniaxial compression", *Comput. Geotech.*, **49**, 206-225. https://doi.org/10.1016/j.compgeo.2012.10.012.

Bahrani, N. and Kaiser, P.K. (2016), "Numerical investigation of the influence of specimen size on the unconfined strength of defected rocks", *Comput. Geotech.*, **77**, 56-67. https://doi.org/10.1016/j.compgeo.2016.04.004.

Capuani, D. and Willis, J.R. (1997), "Wave propagation in elastic media with cracks part I: transient nonlinear response of a single crack", *Eur. J. Mech. A/Solids*, **16**(3), 377-408. https://doi.org/10.1016/S0997-7538(99)80009-6.

Cheng, Y., Song, Z.P., Jin, J.F., Wang, T. and Yang, T.T. (2020a), "Waveform characterisation and energy dissipation of stress wave based on modified SHPB tests", *Geomech. Eng.*, **22**(2), 187-196. https://doi.org/10.12989/gae.2020.22.2.187.

Cheng, Y., Song, Z.P., Chang, X.X. and Wang, T. (2020b), "Energy evolution principles of shock - wave in sandstone under unloading stress", *KSCE J. Civ. Eng.*, **24**(10), 2912-2922. https://doi.org/10.1007/s12205-020-1691-9.

Davies, E.D.H. and Hunter, S.C. (1963), "The dynamics compression testing of solids by the method of the split Hopkinson pressure bar", *J. Mech. Phys. Solids*, **11**(1), 155-179. https://doi.org/10.1016/0022-5096(63)90050-4.

Fan, S.Y., Song, Z.P., Zhang, Y.W. and Liu, N.F. (2020), "Case study of the effect of rainfall infiltration on a tunnel underlying the roadbed slope with weak inter-layer", *KSCE J. Civ. Eng.*, **24**(5), 1607-1619. https://doi.org/10.1007/s12205-020-1165-0.

Hooker, J.N., Ruhl, M., Dickson, A.J., Hansen, L.N., Idiz, E., Hesselbo, S.P. and Cartwright, J. (2019), "Shale anisotropy and natural hydraulic fracture propagation: An example from the Jurassic (Toarcian) posidonienschiefer, Germany", *J. Geophys. Res. Solid Earth*, **125**(3), 2019JB018442. https://doi.org/10.1029/2019JB018442.

Kim, J.S., Kim, G.Y., Baik, M.H. and Cho, G.C. (2019), "A new approach for quantitative damage assessment of in-situ rock mass by acoustic emission", *Geomech. Eng.*, **18**(1), 11-20. https://doi.org/10.12989/gae.2019.18.1.011.

Karma, A. and Lobkovsky, A.E. (2004), "Unsteady crack motion and branching in a phase-field model of brittle fracture", *Phys. Rev. Lett.*, **92**(24), 245510. https://doi.org/10.1103/PhysRevLett.92.245510.

Komoroczi, A., Abe, S. and Urai, J.L. (2013), "Meshless numerical modeling of brittle-viscous deformation: first results on boudinage and hydrofracturing using a coupling of discrete element method (DEM) and smoothed particle hydrodynamics (SPH)", *Comput. Geosci.*, **17**(2), 373-390. https://doi.org/10.1007/s10596-012-9335-x.

Liyanage, P.P., Gamage, R.P. and Xu, T. (2013), "UDEC and RFPA2D simulations on the influence of the geometry of partially-spanning joints on rock mechanical behaviour", Nouvelles Du Collège Deurope, 62-70. http://arrow.monash.edu/vital/access/manager/Repository/monash:1.

Lemaitre, J. (1984), "How to use damage mechanics", *Nucl. Eng. Des.*, **80**(2), 233-245. https://doi.org/10.1016/0029-5493(84)90169-9.

Li, Y.W., Jiang, Y.D., Yang, Y.M., Zhang, H.X., Ren, Z., Li, H.T. and Ma, Z.G. (2016), "Research on loading rate effect of uniaxial compressive strength of coal", *J. Min. Safety Eng.*,

33(4), 754-760. https://doi.org/10.13545/j.cnki.jmse.2016.04.028 (in Chinese).

Li, Y.S. (1995), "Experimental analysis on the mechanical effects of loading rates on red sandstone", *J. Tongji Univ.*, **23**(3), 265-269 (in Chinese).

Qi, C.Z., Wang, M.Y. and Qian, Q.H. (2009), "Strain-rate effects on the strength and fragmentation size of rocks", *Int. J. Impact Eng.*, **36**(12), 1355-1364. https://doi.org/10.1016/j.ijimpeng.2009.04.008.

Mlakar, V., Hassani, F.P. and Momayez, M. (1993), "Crack development and acoustic emission in potash rock", *Int. J. Rock Mech. Min. Sci. Geomech. Abstr.*, **30**(3), 305-319. https://doi.org/10.1016/0148-9062(93)92732-6.

Outer, A.D., Kaashoek, J.F. and Hack, H. (1995), "Difficulties with using continuous fractal theory for discontinuity surfaces", *Int. J. Rock Mech. Min. Sci. Geomech. Abstr.*, **32**(1), 3-9. https://doi.org/10.1016/0148-9062(94)00025-X.

Song, Z.P., Cheng, Y., Tian, X.X., Wang, J.B. and Yang, T.T. (2020), "Mechanical properties of limestone from Maixi tunnel under hydro-mechanical coupling", *Arab. J. Geosci.*, **13**(9), 1-11. https://doi.org/10.1007/s12517-020-05373-z.

Sun, Y. and Yang, Y. (2021), "Energy and fatigue damage evolution of sandstone under different cyclic loading frequencies", *Shock Vib.*, 1-9. https://doi.org/10.1155/2021/5585983.

Stevens, J.L. and Holcomb, D.J. (1980), "A theoretical investigation of the sliding crack model of dilatancy", *J. Geophys. Res.*, **85**(B12), 7091-7100. https://doi.org/10.1029/JB085iB12p07091.

Taheri, A., Zhang, Y.B. and Munoz, H. (2020), "Performance of rock crack stress thresholds determination criteria and investigating strength and confining pressure effects", *Constr. Build. Mater.*, **243**(1), 118263, https://doi.org/10.1016/j.conbuildmat.2020.118263.

Wu, K., Shao, Z.S. and Qin, S. (2020), "An analytical design method for ductile support structures in squeezing tunnels", *Arch. Civ. Mech. Eng.*, **20**(3), 91-101. https://doi.org/10.1007/s43452-020-00096-0.

Wu, K., Shao, Z.S., Qin, S., Zhao, N. and Chu, Z. (2021a), "An improved non-linear creep model for rock applied to tunnel displacement prediction", *Int. J. Appl. Mech.*, **14**, 1-9. https://doi.org/10.1142/S1758825121500958.

Wu, K., Shao Z.S., Qin, S., Wei, W. and Chu, Z. (2021b), "A critical review on the performance of yielding supports in squeezing tunnels", *Tunn. Undergr. Sp. Tech.*, **115**, 103815. https://doi.org/10.1016/j.tust.2021.103815.

Wu, K., Shao, Z.S., Sharifzadeh, M., Hong, S. and Qin, S. (2021c), "Analytical computation of support characteristic curve for circumferential yielding lining in tunnel design", *J. Rock Mech. Geotech. Eng.*, **13**(1), 1-9. https://doi.org/10.1016/j.jrmge.2021.06.001.

Zhao, N., Shao, Z.S., Wu, K., Chu, Z. and Qin, S. (2021), "Time-dependent solutions for lined circular tunnels considering rockbolts reinforcement and face advancement effects", *Int. J. Geomech.*, **21**(10), 04021179. https://doi.org/10.1061/(ASCE)GM.1943-5622.0002130.

Zhou, Y., Su, S.R. and Ma, H.S. (2020), "Experimental research on elastic modulus evolution of chlorite phyllite under cyclic loading", *J. Cent. South Univ. Nat. Sci.*, **51**(3), 783-792 (in Chinese). https://doi.org/10.11817/j.issn.1672-7207.2020.03.024.